Proceedings of the
Annual Stability Conference
Structural Stability Research Council
Louisville, Kentucky, April 13-16, 2021

A system analysis methodology for the practical design of cold-formed steel purlin supported roof systems with paired torsion braces using the Direct Strength Method

Michael W. Seek[1], Onur Avci[2]

Abstract
Cold-formed steel purlins with paired torsion braces rely on the supported sheathing for global stability as the sheathing provides lateral restraint against unsymmetric bending effects and downslope forces. Although conventional design methodologies separately evaluate the strength of cold formed steel purlins and the required system stability forces (anchorage forces), the strength and stability forces are intrinsically related.

A methodology is presented that analyzes the system interaction between a series of purlins within a bay. From the system interaction, geometric second order effects are estimated and the stabilizing forces interacting between the purlins, sheathing and braces are determined. The interacting forces are superimposed on the purlin and a true distribution of cross section stresses from biaxial bending and torsion can be determined. With the true distribution of stresses, the Direct Strength Method is used to determine the global, local and distortional buckling strength at each of the critical locations along the span. The true distribution of stresses can vary significantly from the conventionally assumed constrained bending stress distribution. The provided methodology provides the designer with insights into the system forces and allows the designer to see the influence of system parameters on the strength of the system. The provided methodology better predicts the strength of purlins in sloped roof systems, and in many cases shows strength gains that can be realized by considering the system behavior.

1. Introduction

Paired torsion braces are a popular bracing configuration for cold-formed Z-section roof systems. With this configuration, torsion-only braces are attached to adjacent purlins as shown in Figure 1. These braces are typically located just within the third points of the span. As the name implies, these braces are not laterally anchored and only provide torsional restraint to help to keep the web of the purlin nominally perpendicular to the plane of the roof panels as the Z-section can be subject to substantial torsion. Z-sections, because of their inclined principal axes, when loaded in the plane of their web, will deflect laterally (perpendicular to the plane of the web). Additionally,

[1] Associate Professor, Old Dominion University, <mseek@odu.edu>
[2] Research Assistant Professor, Iowa State University, <oavci@iastate.edu>

with sloped roof systems, downslope forces can be substantial. For the paired torsion bracing configuration, the roof panels resist these forces acting in the plane of the panels. Because the panels are connected to each purlin up the slope, they provide a mechanism to distribute the lateral forces between the purlins, creating a true system behavior.

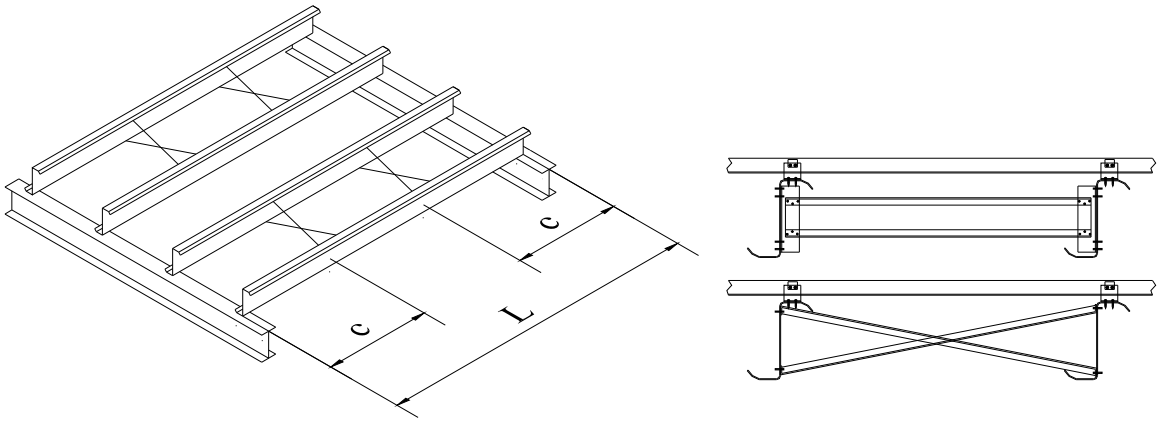

a) Bay layout of torsion braces b) Common torsion brace configurations

Figure 1. Paired torsion braces

Z-section purlin systems are typically used in conjunction with either through-fastened or standing seam panels. Through-fastened panels provide relatively stiff diaphragm and predictable torsional restraint, and the flexural strength of purlins supporting through-fastened panel systems can be predicted by applying a reduction factor derived from testing to the yield moment. For systems of purlins supporting standing seam panels, because the diaphragm is typically much more flexible and the torsional restraint provided by the panels varies greatly from system to system, it is much more difficult to predict the strength of cold-formed purlins in such systems.

The industry therefore relies on the base test AISI (2017a) to determine the strength of purlins supporting standing seam systems. In the base test, a pair of purlins in a simple span configuration is topped with panels and subjected to a uniform pressure by creating a pressure differential with a vacuum chamber. Based on the results of the base test, similar to the through-fastened systems, a reduction factor is applied to the yield moment. This reduction factor is specific to the purlin cross section, panel type, and clip typed used in the test. Therefore, for each different combination of purlin, panel and clip, a separate series of tests must be performed.

For a system of purlins with paired torsion braces, Seek et. al. (2016) showed that displacement compatibility could be used to predict the forces interacting between the purlins, standing seam panels, and braces. With these forces superimposed on the purlin, biaxial bending and torsion cross section stresses can be determined at critical locations along the span of the purlin. These stresses can vary significantly from the traditionally assumed constrained bending stress distribution used as a basis to predict the strength. With an actual distribution of stresses on the cross section, the Direct Strength Method can be used to predict the strength of the purlin. When applied to a series of base tests on purlins with paired torsion braces, this method was shown to predict the strength as well as predict failures away from the brace at the mid-span.

There are substantial differences between purlins in a base test versus purlins in a real roof system. The biggest difference between the two is slope: in a real roof system, the downslope forces can substantially affect the deformation of the diaphragm and thus the stresses in the purlins. Additionally, in a real roof system, all purlins may not be subject to the same loading along their span. Because the panels connect each purlin in a bay to create a system, these uneven forces are redistributed in-plane by the diaphragm. To expand the methodology developed by Seek (2018) for base tests to real systems, modifications are made to account for slope effects and the redistribution of forces.

The methodology explained herein is demonstrated in a detailed example in Seek (2020)

2. Displacement compatibility to determine system forces

To analyze a system of purlins, the starting point is to determine the forces interacting between the purlins and the diaphragm created by the panels. This methodology can be used for both C-sections and Z-sections individually or with them combined in the same bay, as is common to use a C-section eave strut in combination with Z-section purlins in the rest of the field. Because of the inclined principal axes of the Z-section, the lateral restraining forces in the diaphragm can be significant. The system of purlins and diaphragm are approximated as a single degree of freedom system. The purlins are considered linked together by the panels at the torsional brace location. There are some limitations to this approximation discussed later. For this single degree of freedom system, there are two forces driving the lateral displacement of the diaphragm: the unsymmetric bending forces as a result of the inclined principal axes of the z-section and the downslope forces resulting from the roof slope. Resisting these forces are the weak axis bending strength of the purlins and the diaphragm resistance of the panels. By simplifying the system as a single degree of freedom system, the lateral deformation (in the plane of the panels) of the system, Δ, can be determined from a simple summation of the forces for each purlin in the bay being analyzed.

$$\Delta_{brace}, \Delta_{mid} = \frac{\sum\left(w_y L \frac{I_{xy}}{I_x}\alpha\right)_i + \sum w_{x,i} L}{\sum\left(\frac{E \cdot I_{my}}{C_1 L^3}\right)_i + \frac{G' Bay}{C_2 L}} = \frac{\sum\left(w_y L \frac{I_{xy}}{I_x}\alpha\right)_i + \sum w_{x,i} L}{\sum\left(k_{purlin}\right)_i + k_{diaph}} \quad (1)$$

where

Bay = total depth of the diaphragm
G' = diaphragm stiffness
I_x = moment of inertia about the orthogonal x-axis
I_{xy} = product of inertial relative to the orthogonal axis
I_{my} = modified moment of inertia about the orthogonal y-axis
$= \frac{I_x I_y - I_{xy}^2}{I_x}$
L = purlin span
w_y = load parallel to the web
w_x = downslope load in plane of sheathing

α_i = defines the orientation of the purlin
= 1 for top flange facing upslope
= -1 for top flange facing downslope

Coefficients C_1 and C_2 are derived from the purlin bending displacement and the diaphragm shear displacement, respectively as a result of a uniform load along the purlin span. The deformation of the system is calculated at the brace location to estimate the forces interacting between the purlin and the sheathing and at mid-span to estimate second order torsions induced on the purlin. For each location, a separate coefficient must be calculated. The coefficient C_1 varies according to the span condition, whereas the coefficient C_2 is the same for all span configurations. For example, for a multi-span purlin system that is approximated with fixed-fixed end conditions and symmetric braces located at distance c from the end, coefficients at the brace location are

$$C_{1,brace} = \frac{1}{24} \cdot \left(\frac{c}{L}\right)^2 \cdot \left(1 - \frac{c}{L}\right)^2 \tag{2}$$

$$C_{2,brace} = \frac{1}{2} \cdot \left(\frac{c}{L}\right) \cdot \left[1 - \left(\frac{c}{L}\right)\right] \tag{3}$$

Similarly, at the mid-span of the purlin, the coefficients are

$$C_{1,mid} = \frac{1}{24} \cdot \left(\frac{1}{2}\right)^2 \cdot \left(1 - \frac{1}{2}\right)^2 = \frac{1}{384} \tag{4}$$

$$C_{2,mid} = \frac{1}{2} \cdot \left(\frac{1}{2}\right) \cdot \left[1 - \left(\frac{1}{2}\right)\right] = \frac{1}{8} \tag{5}$$

Coefficients C_1 and C_2 can be similarly derived for other span configurations (simple-span end bay, multi-span interior bay, etc.) and are presented in Seek (2020).

Once the lateral deformation of the system at the brace is determined, the lateral force acting between the purlin and the sheathing, w_{rest} can be determined.

$$w_{rest,i} = \left(w_{y,i} \frac{I_{xy}}{I_x} \alpha_i - \frac{\Delta_{brace} \cdot E \cdot I_{my,i}}{C_{1,brace} L^4} \right) \alpha_i \tag{6}$$

For simplification in calculations, the proportion of the applied force parallel to the web of the purlin that is transferred to the horizontal force in the diaphragm for each purlin, ρ_i, is calculated

$$\rho_i = \frac{w_{rest,i}}{w_{y,i}} \tag{7}$$

If a system of purlins is largely uniform, that is each purlin along the slope of the roof utilizes the same cross section, same orientation and has the same loading, this uniform restraint force will be essentially the same. However, as loads or spacing may vary between purlin lines (for example an unbalanced snow load at the ridge), as a different purlin is used at the eave (as is common to use a different eave strut), or as the orientation of some of the purlins may change (top flange facing downslope), the uniform restraint force for different purlins may vary significantly. This is an indication of the system's ability to redistribute the lateral forces.

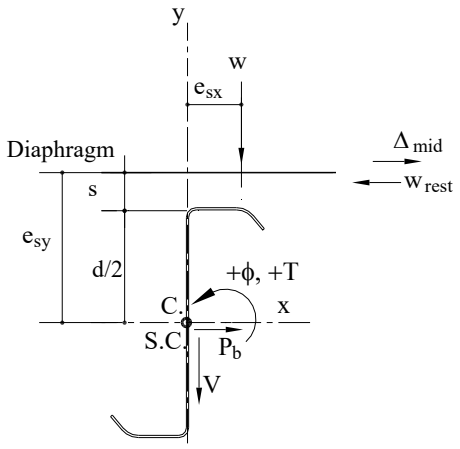

Figure 2. Positive directions for axes, forces and deflections

The lateral force acting between the purlin and the sheathing is critical because it imparts a substantial torsion on the purlin which in turn must be resisted by the torsion braces. This lateral force acts above the top flange of the purlin at the effective standoff distance, s, defined in AISI (2018), resulting in a net eccentricity from the shear center, e_{sy} as shown in Figure 2. Additionally, the applied force perpendicular to the panels acts at an eccentricity, e_{sx}, along the flange of the purlin, inducing additional torsion. These two effects combine to create a first order (primary) uniform torsion along the length of each purlin, $t_{1st,i}$

$$t_{1st,i} = \left(w_{y,i}\right)\left(\rho_i \cdot e_{sy,i} - e_{sx,i}\right) \tag{8}$$

As the system of purlins deflects laterally (perpendicular to the web of the purlin) with the panels, additional second order torsional moments are applied to the purlins. These moments are approximated to have a parabolic distribution along the length of the purlin with the peak moment, t_{2nd}, proportional to the mid-span lateral deflection of the panels.

$$t_{2nd,i} = -\left(\alpha_i w_{y,i}\right)\Delta_{mid} \tag{9}$$

As previously noted, the distributed torsions along the length of the purlin can be significant. If left unchecked, the torsional deformations would greatly reduce the load carrying capacity of the purlins. Applying paired torsional braces therefore is an effective strategy to minimize the torsional deformations of the purlin. The paired torsion braces apply concentrated torques T_{1st} and T_{2nd}, to the purlin that counteract the distributed torsion effects, t_{1st}, and t_{2nd} respectively.

$$T_{1st,i} = -(C_3)\, t_{1st,i} L \tag{10}$$

$$T_{2nd,i} = -(C_4)\, t_{2nd,i} L \tag{11}$$

The coefficients C_3 and C_4 are determined from torsional displacement compatibility of the purlin at the brace location. In other words, T_{1st} and T_{2nd} are the respective concentrated brace torsion moments required to restore the torsional rotation from the distributed torsion to zero. The braces are approximated to be rigid. When considering displacement compatibility, because warping torsion dominates the behavior, pure (St. Venant's) torsion is ignored. This approximation yields negligible differences in the brace forces. For example, a simple span purlin with braces at distance, c, from the supports has coefficients C_3 and C_4

$$C_3 = \frac{1}{4} \cdot \frac{\left(1 - \frac{c}{L}\right)^2}{\left(\frac{c}{L}\right)\left(2 - 3\frac{c}{L}\right)} \tag{12}$$

$$C_4 = \frac{1}{15} \cdot \frac{3 - 5\left(\frac{c}{L}\right) + 3\left(\frac{c}{L}\right)^3 - \left(\frac{c}{L}\right)^4}{2\left(\frac{c}{L}\right) - 3\left(\frac{c}{L}\right)^2} \tag{13}$$

Coefficients for additional span configurations are presented in Seek (2020).

As moments are developed at each end of the torsion braces, to balance the moments, shear forces at each end of the brace are developed and must be resisted by the purlins as shown in Figure 3. These shear forces of course affect the strong axis bending moments in the purlin and must be accounted for. The shear force at the end of each brace, V, is calculated by

$$V_i = -\frac{\left(\sum T_i \alpha_i\right)}{spa} \xi_i \tag{14}$$

Where

Downslope purlin $\xi = 1$

Upslope purlin $\xi = -1$

As the brace shear forces are applied to the purlin, a small axial force, P_b, is generated in the brace as a result of the unsymmetric bending of the purlin. Because the shear forces are typically equal and opposite at each end of brace, so too the brace axial force is considered to be equal and opposite. Depending on the direction of the brace moments, the axial force in the brace can either be tensile or compressive.

$$P_{b,i} = -V_i \alpha_i \frac{I_{xy,i}}{I_{x,i}} \tag{15}$$

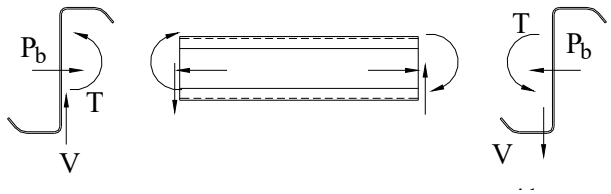

Figure 3. Shear forces to balance torsion brace moments

3. Cross Section Stresses

The forces and moments acting on the purlin are superimposed to calculate the cross- section stresses. Biaxial bending stresses and torsion stresses are evaluated independently, then superimposed on the purlin cross section.

Biaxial Bending Stresses

For convenience, the moments in the purlin cross section are evaluated on the orthogonal x- and y- axes perpendicular and parallel respectively to the web of the purlin. The purlin is subject to moments about the x-axis due to uniformly distributed loads, $M_{x,dist}$, and the brace shear forces, $M_{x,V}$, as well as moments about the y-axis, M_y, as a result of forces generated in the panels, M_y. Because the diaphragm forces in the panel are proportional to the applied uniform forces by the factor of ρ, so too M_y is proportional to $M_{x,dist}$.

$$M_y = M_{x,dist} \cdot \rho \tag{16}$$

The bending stresses, f_b, are mapped to x and y coordinates along the cross section according to

$$f_b = M_{x,dist}\left[\frac{-y}{I_{mx}} + \frac{x\frac{I_{xy}}{I_x}}{I_{my}}\right] + M_{x,V}\left(\frac{-y}{I_x}\right) + M_y\left[-\frac{x}{I_{my}} + \frac{y\frac{I_{xy}}{I_y}}{I_{mx}}\right] \tag{17}$$

Because the x- and y-axes rotated from the principal axes, the cross section bending stresses resulting from the uniformly distributed loads are calculated using the modified moments of inertia proposed by Zetlin and Winter (1955).

$$I_{mx} = \frac{I_x I_y - I_{xy}^2}{I_y} \tag{18}$$

$$I_{my} = \frac{I_x I_y - I_{xy}^2}{I_x} \tag{19}$$

For the moment generated from the brace shear force, $M_{x,V}$, because an axial brace force accompanies the brace shear force, the stresses resulting from this effect conform to a constrained bending stress distribution and are determined by the more conventional bending formula $M(y)/I_x$.

Torsion Stresses

Warping torsion normal stresses, f_w are calculated as presented in the AISC Torsion Analysis Design Guide (Seaburg and Carter, 1997) considering both pure torsion and warping torsion resistance

$$f_w = E \cdot W_N \cdot \left(\phi_u'' + \phi_p'' + \phi_{brace}''\right) \tag{20}$$

where W_N is the normalized warping function at a specific point on the cross section and ϕ'' is the second derivative of the rotation function with respect to z due to the applied load. The rotation functions correspond to the torsional load effects: uniform torsion, ϕ_u'', parabolic distributed torsion, ϕ_p'', and concentrated torque at the brace location, ϕ_{brace}''. These rotation functions are derived for the simple span condition (torsion fixed, warping free), multi-span end bay (torsion fixed, warping free / torsion fixed, warping fixed) and the multi-span interior bay condition (torsion fixed, warping fixed) in Seek (2020). For a multi-span interior bay, the second derivatives of the rotation functions are

Uniform torsion

$$\phi_u'' = \frac{t_{1st}}{GJ}\left(\left(\frac{L}{2a}\right)\left(\frac{\cosh\left(\frac{L}{2a}\right)}{\sinh\left(\frac{L}{2a}\right)}\right)\cosh\left(\frac{z}{a}\right) - \left(\frac{L}{2a}\right)\sinh\left(\frac{z}{a}\right) - 1\right) \tag{21}$$

Parabolic torsion

$$\phi_p'' = \frac{t_{2nd}}{GJ}\left[\frac{L}{a}\left(\frac{1}{3} - \frac{4a^2}{L^2}\right)\left(\frac{\cosh\left(\frac{L}{2a}\right)}{\sinh\left(\frac{L}{2a}\right)}\cosh\left(\frac{z}{a}\right) - \sinh\left(\frac{z}{a}\right) + 1\right) + 4\left(\frac{z}{L}\right)^2 - 4\left(\frac{z}{L}\right) + \frac{8a^2}{L^2}\right] \tag{22}$$

Concentrated brace torque

$z < c$

$$\phi_{brace}'' = \frac{T}{GJ}\left(\frac{1}{a}\right)\left(\left(\frac{\cosh\left(\frac{L}{2a}\right)}{\sinh\left(\frac{L}{2a}\right)}\left(1 - \cosh\left(\frac{c}{a}\right)\right) + \sin h\left(\frac{c}{a}\right)\right)\cosh\left(\frac{z}{a}\right) - \sinh\left(\frac{z}{a}\right)\right) \tag{23}$$

$c < z < (L-c)$

$$\phi_{brace}'' = \frac{T}{GJ}\left(\frac{1}{a}\right)\left(1 - \cosh\left(\frac{c}{a}\right)\right)\left(\frac{\cosh\left(\frac{L}{2a}\right)}{\sinh\left(\frac{L}{2a}\right)}\cosh\left(\frac{z}{a}\right) - \sinh\left(\frac{z}{a}\right)\right) \tag{24}$$

4. Calculation of Flexural Strength

Stresses are analyzed at each of the critical flexural locations along the span of the purlin. These critical locations include the lapped purlins at the support, the single purlin at the end of the lap, the unbraced purlin between the braces. At each critical location, the flexural and torsion stresses are superimposed across the cross section to find the true distribution of stresses. The maximum tensile (+) and compressive (-) stresses across the cross section are determined. All of the stresses in the cross section are then scaled by the ratio of the yield stress to the maximum absolute value stress, thus setting the stresses to the point of first yield. With the scaled stresses, a finite strip buckling analysis is performed. An example of a true stress distribution is shown in Figure 4. From this stress distribution, it can be seen that the lateral bending and torsion effects are significant and that the stress distribution is significantly different than the typically assumed constrained bending stress distribution.

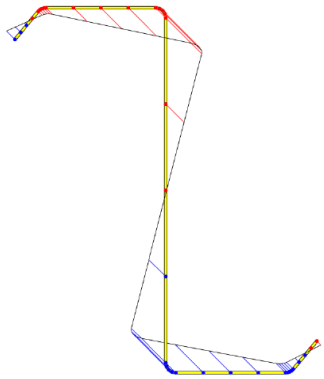

Figure 4. Stress distribution with biaxial bending and torsion

Global buckling analysis

For global buckling, foundation springs representing the lateral (diaphragm) restraint, $k_{lateral}$, and rotational restraint, k_ϕ, provided by the panels are included. For local and distortional modes, no restraint from the panels is included because the length of the buckling half-wave of these modes is much shorter than the clip spacing. The foundation springs used for global buckling analysis are applied at the intersection of the top flange and the flange-web radius. The rotational stiffness of the purlin to clip connection, k_ϕ can be determined by the test standard AISI S901-17 (AISI 2017a) and a range of values for common clip types are provided in AISI (2018). The lateral stiffness, $k_{lateral}$, is derived from the diaphragm stiffness, G', and is calculated according to the length of the purlins between brace locations, L_{brace}, and the diaphragm width tributary to the purlin (approximated by the purlin spacing, b_{purlin_space})

$$k_{lateral} = \frac{8G'\left(b_{purlin\ space}\right)}{L_{brace}^2} \tag{25}$$

The finite strip buckling analysis can be performed using CUFSM (Li and Schafer, 2010)
. Along the unbraced length of the purlin, the stress distributions may vary, therefore analysis may need to be performed at multiple locations. Conservatively, a bending modification coefficient of C_b = 1.0 can be used. This may be very conservative for some situations,

particularly towards the ends of the span. More research is needed, but in the interim this provides a conservative approach. In general, with the inclusion of the lateral and rotational springs, for reasonably proportioned systems, the global buckling strength doesn't control or only has a small impact. A sample output from CUFSM (signature curve) of the global buckling analysis is shown in Figure 5. The signature curve provides the buckling load coefficient chosen from the unbraced length. From the example in the figure, the unbraced length was 84 in. resulting in a buckling load coefficient of 2.02.

Local and distortional buckling analysis

Similarly, to determine the distortional and local buckling strength, a finite strip buckling analysis is performed with the stress distribution according to the analysis location and as mentioned previously, without the sheathing spring restraints. An example signature curve from this analysis is provided in Figure 6. Note that there is very little difference between this curve and the one for the global buckling analysis except for the longer wavelengths, indicating that the panel restraints have very little impact on the local and distortional buckling strength. From the example signature curve, the local buckling load factor at a half-wavelength of 5 in. 0.68 and the distortional buckling load factor is 0.99 at a half-wavelength of 30 in.

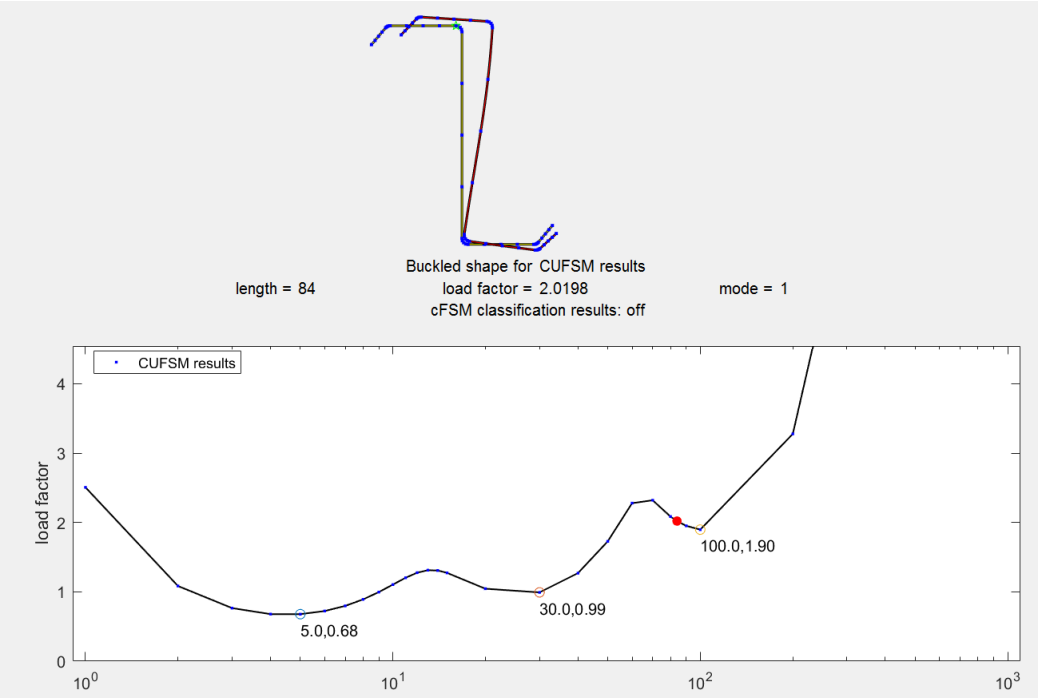

Figure 5. Global buckling signature curve (with spring restraints)

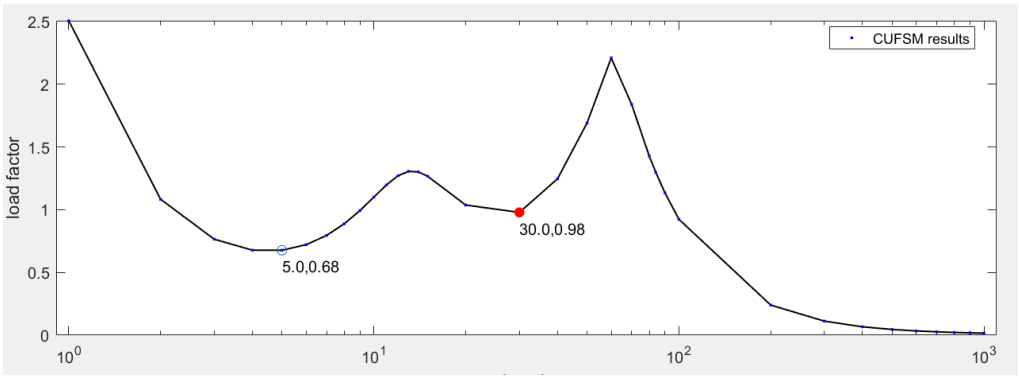

Figure 6. Local and distortional buckling signature curve

Nominal Flexural Strength

For each of the critical location, once the buckling load factors for global, local, and distortional buckling are determined, the strength of the cross section is determined according to AISI S100 (2016). Strength comparison is determined for moments about the x-axis. The required moment about the x-axis, M_x, is the sum of the uniformly distributed moment, $M_{x,dist}$, and the brace shear force moment, $M_{x,V}$ at each analysis location. The moment about the x-axis is multiplied by the stress scale factor to determine the yield moment M_{yield}. Because the initial stress distribution includes biaxial bending and torsion, these effects are essentially scaled by the same factor. The global buckling nominal strength is calculated according to AISI S100 section F2.1. based on a critical global buckling moment, M_{cre} equal to

$$M_{cre} = M_{yield} \cdot \text{(LTB buckling load factor)} \tag{26}$$

Similarly, the strength of local buckling interacting with global buckling, $M_{n\ell}$, is determined according to AISI S100 Section F3.2.1. with the critical local buckling moment, $M_{nr\ell}$, equal to the product of M_{yield} and the local buckling load factor. Finally, the distortional buckling strength, M_{nd}, is determined according to AISI S100 section F4.1 based on a critical distortional buckling moment , M_{nd}, equal to the product of M_{yield} and the distortional buckling load factor.

The nominal flexural strength at each analysis location along the length of the beam, M_n, is the minimum of the global, local, and distortional buckling strength at that location. It should be noted that because the distributions of stresses changes at different locations along the length of the beam, the predicted nominal strength will vary at different locations as well. The nominal strength at each critical section is compared to the required moment, M_x, at the section by taking the ratio of the required moment to the nominal moment. The location with the highest ratio of required moment to nominal moment strength controls the capacity of the purlin. Provided that at each location this ratio is less than unity, the member has sufficient strength to resist the applied loads.

Although strength is only checked relative to the x-axis, because the buckling load factors are determined according to a stress distribution that incorporates biaxial bending and torsion, these effects are incorporated into the predicted strength about the x-axis. The process is essentially a direct analysis approach. Stresses and second order effects are determined according to a specific applied load, and thus the predicted strength corresponds to that applied load. As long as the

required strength is less than the predicted strength, then the system has the capacity to support the applied loads. As applied loads are increased, second order effects also increase, which changes the distribution of stresses. Therefore, if it is desired to determine the maximum strength (the magnitude of the load that would cause failure), some iteration would be required until the nominal strength matched the required strength.

Once the initial system analysis is performed to determine the lateral deformation of the system of purlins, the strength analysis is performed on a purlin-by-purlin basis. However, if a change is made to any of the purlins (for example, if the size is changed for one of the purlins in the system), the system analysis would need to be re-run.

5. Summary of System Interaction

To summarize the process to evaluate the interaction of purlins, the first step is to first calculate the overall lateral deflection of the system of purlins, Δ, approximated from a single degree of freedom system. From the lateral deflection, the lateral force interacting between each purlin and the panels, w_{rest}, is determined. For each purlin, the lateral restraint force from the sheathing drives the first order uniform torsion induced on the purlin, t_{1st}, and the approximate second order torsion, t_{2nd}, is proportional to the mid-span lateral deflection. The paired torsion braces apply concentrated brace torques, T_{1st} and T_{2nd}, to limit the torsional deformation of the purlin. To balance the moments generated in the torsion braces, shear forces are developed at the end of each brace and imparted to the purlins.

All of the forces in the system are linked to the lateral deflection of the system. Thus, changes to the lateral deflection of the system trickle down through all the forces interacting with the system. Previous methods to quantify the system forces as outlined in Seek (2018) evaluate each purlin (or pair of purlins) in a system individually. This approximation works well for a system of purlins where all purlins in a bay are the same cross section with the same spacing and loaded equally.

The system analysis approach also intrinsically links the provided strength of the system of purlins with the restraint provided by the sheathing and braces. Historically, the strength of the system and the restraining forces of the braces and sheathing have been analyzed separately. With the provided approach, the restraining forces of the system are calculated directly as part of the analysis. Changes to the system restraint will have measurable impacts to the strength of the system, as should be expected.

However, as a bay of purlins becomes less uniform it becomes necessary to evaluate the system holistically to better predict the behavior. It is common for a bay of purlins to have a different purlin at the eave (eave strut), and nonuniform loading along the slope (larger loads at the eave or ridge). Additionally, while most purlins typically have the top flange facing upslope, some systems may utilize a portion of the purlins facing downslope. These downslope facing purlins can be accommodated with the purlin orientation factor, α. The panels connected between each purlin in the bay provides a pathway to help the purlins share and redistribute the lateral forces between parallel purlin lines. This redistribution of forces in general improves the overall capacity of the purlins.

There are some limitations to analyzing the system of purlins as a single degree of freedom system. Many standing seam systems utilize an articulating clip that allows for relative lateral movement between the purlin and the sheathing to accommodate thermal expansion and contraction of the system. Even standing seam systems with "fixed" clips may allow some lateral movement between the purlin and panels as well. Some of this slippage is captured in the diaphragm stiffness, G', used to calculate the deformation of the system. However, when relative lateral movement occurs between the purlin and the panel, using a single degree of freedom for the system does not approximate the behavior as well. This relative slip between a purlin and panel reduces the panels ability to redistribute forces. It is expected, however that this relative movement will generally reduce the predicted forces required of the diaphragm to redistribute forces. To truly capture this relative slip between the panel and purlin would require analyzing each purlin in the system with multiple degrees of freedom along the length of each. This increases the complexity of the required analysis. Additionally, the slip between the panel and purlin has not been well quantified. It is presumed to be dependent upon the applied gravity or uplift load and is likely highly non-linear.

Another limitation of the single degree of freedom system presented here is that it is based on purlins uniformly loaded along their length. Wind loads and unbalanced snow loads can produce varying loads along the length of the purlin. Approximations can be made with a single degree of freedom system but to better accommodate this behavior would require a much more complex multi-degree of freedom system analysis.

While analyzing the system with a single degree of freedom has its limitations, the provided methodology provides a good starting point to investigate the complex interaction between a system of purlins, the panels and braces. It provides valuable insight into the potential effects changes to one component of the system may have on other components. While a more detailed analysis may yield a more refined result, the provided methodology provides a conservative result and balances computational complexity with design efficiency for these very complex and varied systems.

6. Conclusions

A method is provided for analyzing a system of purlins within a bay using the Direct Strength Method. Sheathing connected between lines of purlins within a bay facilitates sharing of lateral forces between the system of purlins. Approximating the system as a single degree of freedom system, the overall lateral deformation can be calculated, geometric second order effects can be approximated, and the forces interacting between the purlin, sheathing and braces can be determined. From the system forces, the biaxial bending stresses and warping torsion normal stresses may be determined at critical locations along the span of the purlin. With the actual distribution of cross section stresses, the Direct Strength Method is used to determine the nominal global, local, and distortional buckling strength relative to bending about the x-axis. While only the strength about the x-axis is checked, because the distribution of stresses incorporates biaxial bending and torsion, these effects are incorporated into the analysis. Rather than calculate the nominal strength of each of these effects, a check is simply made to ensure that for the loads applied, buckling will not occur. This strength check yields conservative results, as a more detailed analysis considering inelastic reserve capacity may provide greater predicted capacity.

By analyzing the system of purlins truly as a system, the forces interacting between purlins in the same bay can be analyzed. The effects of changing the size or orientation of even one purlin in the system has the potential to impact the strength of all of the purlins in the system. The provided methodology provides a mechanism for the user to analyze the effects of these changes. The system is approximated with a single degree of freedom, which has its limitations for incorporating the complex behavior of the clip connecting a purlin to a standing seam panel and non-uniform loads. While simplified, it greatly improves upon current methodologies to analyze purlin supported roof systems.

References

AISI (American Iron and Steel Institute) (2016) *S100-16 North American Specification for the Design of Cold-Formed Steel Structural Members*. AISI. Washington, DC. 2016.

AISI (American Iron and Steel Institute) (2017a) S901-17 *Rotational-Lateral Stiffness Test Method for Beam-to-Panel Assemblies*. AISI. Washington, DC. 2017.

AISI (American Iron and Steel Institute) (2017c). S908-17 *Base Test Method for Purlins Supporting a Standing Seam Roof System*. AISI. Washington, DC. 2017.

AISI (American Iron and Steel Institute) (2018). Research Report RP18-3 *Determination of Effective Standoff in Standing Seam Roof Systems.* AISI. Washington, DC. 2018.

AISI (American Iron and Steel Institute) (2019). Research Report RP19-3 *Direct Strength Prediction of Purlins with Paired Torsion Bracing.* AISI. Washington, DC. 2018.

Li, A., Schafer, B.W. (2010) "Buckling analysis of cold-formed steel members with general boundary conditions using CUFSM: conventional and constrained finite strip methods." *Proceedings of the 20th International Specialty Conference on Cold-Formed Steel Structures.* 2010.

Seaburg, P. A., Carter, C. J. (1997) *Steel Design Guide Series 9: Torsional Analysis of Structural Steel Members*. American Institute of Steel Construction. Chicago, IL. 1997.

Seek, M.W., Ramseyer, C. and Kaplan, I. (2016). "A Combined Direct Analysis and Direct Strength Approach to Predict the Flexural Strength of Z-Purlins with Paired Torsion Braces". *Proceedings of the 23rd International Specialty Conference on Cold-Formed Steel Structures.* 2016.

Seek, M.W. (2018). "Flexural Strength of continuous-span Z-purlins with paired torsion braces using the Direct Strength Method". *Proceedings of the 24th International Specialty Conference on Cold-Formed Steel Structures.* 2018.

Seek, M.W. (2020). *A Direct Strength design example for purlin supported roof systems with paired torsion bracing.* Metal Building Manufacturers Association, Columbus, OH. 2020.

Zetlin, L and G. Winter. (1955). "Unsymmetrical Bending of Beams with and without Lateral Bracing." Journal of the Structural Division, ASCE, Vol. 81, 1955.